Global Warming–Induced Changes in El Niño Teleconnections over the North Pacific and North America

ZHEN-QIANG ZHOU

Physical Oceanography Laboratory/Qingdao Collaborative Innovation Center of Marine Science and Technology, Key Laboratory of Ocean–Atmosphere Interaction and Climate in Universities of Shandong, Ocean University of China, Qingdao, China

SHANG-PING XIE

Physical Oceanography Laboratory/Qingdao Collaborative Innovation Center of Marine Science and Technology, Key Laboratory of Ocean–Atmosphere Interaction and Climate in Universities of Shandong, Ocean University of China, Qingdao, China, and Scripps Institution of Oceanography, University of California at San Diego, La Jolla, California

XIAO-TONG ZHENG, QINYU LIU, AND HAI WANG

Physical Oceanography Laboratory/Qingdao Collaborative Innovation Center of Marine Science and Technology, Key Laboratory of Ocean–Atmosphere Interaction and Climate in Universities of Shandong, Ocean University of China, Qingdao, China

(Manuscript received 3 April 2014, in final form 11 September 2014)

ABSTRACT

El Niño–Southern Oscillation (ENSO) induces climate anomalies around the globe. Atmospheric general circulation model simulations are used to investigate how ENSO-induced teleconnection patterns during boreal winter might change in response to global warming in the Pacific–North American sector. As models disagree on changes in the amplitude and spatial pattern of ENSO in response to global warming, for simplicity the same sea surface temperature (SST) pattern of ENSO is prescribed before and after the climate warming. In a warmer climate, precipitation anomalies intensify and move eastward over the equatorial Pacific during El Niño because the enhanced mean SST warming reduces the barrier to deep convection in the eastern basin. Associated with the eastward shift of tropical convective anomalies, the ENSO-forced Pacific–North American (PNA) teleconnection pattern moves eastward and intensifies under the climate warming. By contrast, the PNA mode of atmospheric internal variability remains largely unchanged in pattern, suggesting the importance of tropical convection in shifting atmospheric teleconnections. As the ENSO-induced PNA pattern shifts eastward, rainfall anomalies are expected to intensify on the west coast of North America, and the El Niño–induced surface warming to expand eastward and occupy all of northern North America. The spatial pattern of the mean SST warming affects changes in ENSO teleconnections. The teleconnection changes are larger with patterned mean warming than in an idealized case where the spatially uniform warming is prescribed in the mean state. The results herein suggest that the eastward-shifted PNA pattern is a robust change to be expected in the future, independent of the uncertainty in changes of ENSO itself.

1. Introduction

El Niño–Southern Oscillation (ENSO), the leading mode of interannual climate variability in the tropical Pacific, has profound impacts on global weather and climate (Philander 1990; Hoerling et al.1997; McPhaden et al. 2006; Collins et al. 2010; Deser et al. 2010; Cai et al. 2011). ENSO teleconnections illustrate that sea surface temperature (SST) anomalies in the equatorial Pacific have substantial remote effects on climate around the globe (Horel and Wallace 1981; Trenberth 1997; Wallace et al. 1998). Previous studies suggested that ENSO teleconnections might change in response to global warming (Meehl and Teng 2007; Kug et al. 2010; Stevenson 2012). The Intergovernmental Panel on Climate Change (IPCC) Fifth

Corresponding author address: Shang-Ping Xie, Scripps Institution of Oceanography, University of California at San Diego, 9500 Gilman Drive, MC 206, La Jolla, CA 92093-0206.
E-mail: sxie@ucsd.edu

DOI: 10.1175/JCLI-D-14-00254.1

Assessment Report alluded to a possible eastward shift of the ENSO-induced Pacific–North American (PNA) teleconnection pattern (Christensen et al. 2013).

Considerable disagreements remain among climate models with regard to global warming–induced changes in ENSO teleconnections (Meehl and Teng 2007; Kug et al. 2010; Stevenson 2012) for a number of reasons. Coupled ocean–atmosphere models disagree on changes in ENSO amplitude and spatial structure in SST in response to global warming (Collins et al. 2010; Christensen et al. 2013). These ENSO properties (Wittenberg 2009; Li et al. 2013; Ogata et al. 2013) and the PNA pattern (Deser et al. 2012) both display large internal variability that is hard to distinguish from the forced response in single model runs. Here, we sidestep these issues and focus on the following question. Would there be robust changes in ENSO-induced atmospheric anomalies in a warmer climate if the SST pattern of ENSO remained the same? Recent studies identified systematic changes in tropical rainfall response to ENSO that are insensitive to changes in ENSO pattern of SST (Power et al. 2013; Cai et al. 2014). We extend these studies by looking into atmospheric response in both the tropics and midlatitudes.

Changes in the mean state are important for changes in ENSO. In addition to a spatially uniform component in response to anthropogenic radiative forcing, the ocean warming displays pronounced spatial variations (Xie et al. 2010). For example, the SST warming peaks on the equator in the tropical Pacific due to reduced evaporative damping. Changes in tropical convection are strongly influenced by SST spatial structure (Xie et al. 2010; Chadwick et al. 2013; Chung et al. 2014; Ma and Xie 2013; Huang et al. 2013). In the warmer-get-wetter hypothesis, tropical rainfall shifts to regions with large SST increases (relative to the tropical-mean warming). Although changes in ENSO amplitude and spatial structure are uncertain in coupled ocean–atmosphere model projections (e.g., Collins et al. 2010; Power et al. 2013), robust changes in the spatial pattern of ENSO-driven variability in tropical precipitation emerge in coupled model projections. During El Niño, the precipitation response intensifies in the central to eastern tropical Pacific with a drying in the Maritime Continent and western Pacific (Kug et al. 2010; Chung et al. 2014; Power et al. 2013), due to the equatorial peak in the mean warming (Cai et al. 2014). These changes represent an intensification and eastward shift of El Niño–induced convective anomalies in the tropical Pacific under global warming, conceivably affecting ENSO teleconnections into the extratropics.

Power et al. (2013) showed that SST-forced atmospheric general circulation model (AGCM) results in this context could mimic important aspects of the changes evident in the multimodel mean of phases 3 and 5 of the Coupled Model Intercomparison Project (CMIP3 and CMIP5, respectively), and that radiative changes played a secondary role in driving precipitation changes over the ocean. Chung et al. (2014) showed that the SST-forced response depends on the spatial structure of the imposed SST warming in the mean state. These studies indicate that SST-forced AGCM results can shed light on how ENSO (an inherently coupled phenomenon) and its teleconnections might change under global warming.

The present study examines ENSO teleconnection changes under global warming and investigates the underpinning dynamical mechanisms, with an emphasis in the Pacific–North American sector during winter [December–February (DJF)]. Deviating from previous studies using coupled models, we sidestep the uncertainties in ENSO amplitude and pattern by imposing an El Niño composite of SST anomalies based on observations in the Community Atmosphere Model, version 4 (CAM4), in two separate time slices, one for the present and one for a warmer future climate. The use of the identical El Niño composite enables us to isolate atmospheric processes for teleconnection changes between the present and future simulations. Another benefit of using an AGCM is that we can investigate the effect of the SST warming pattern by specifying either a spatially uniform SST increase (SUSI) or spatially patterned SST increase (SPSI) in the mean state for the future. We show that the model simulates an intensification and eastward shift in El Niño–induced tropical rainfall anomalies and the PNA pattern, and that these changes in atmospheric anomalies of El Niño are more pronounced for SPSI than SUSI, implicating the importance of SST warming pattern for interannual variability. In addition to the SST-forced experiments with CAM4, we also examine SST-forced results from 11 AGCMs made available through CMIP5 of the World Climate Research Programme (WCRP). Finally, we analyze ENSO teleconnection changes in observations between epochs of an anomalously warm and cold tropical Pacific.

The rest of the paper is organized as follows. Section 2 briefly describes the datasets, methods, and SST-forced experiments. Sections 3 and 4 examine ENSO teleconnection changes under different global warming (SST) scenarios in CAM4 and the 11-AGCM multimodel ensemble from CMIP5, respectively. Section 5 discusses ENSO teleconnection changes in observations. Section 6 is a summary and discussion.

2. Datasets and methods

a. Observations

We analyze observational data to validate our model results. For SST, we use the Extended Reconstructed

TABLE 1. Summary of CAM4 experiments; the subscript ctrl refers to the control run, clim to climatology, and EN to El Niño.

Name	Prescribed SST	Ensemble	Length (yr)
$\text{Present}_{\text{ctrl}}$	SST_{clim}	1	50
$\text{Present}_{\text{EN}}$	$\text{SST}_{\text{clim}} + \text{SST}_{\text{EN}}$	20	2
$\text{SUSI}_{\text{ctrl}}$	$\text{SST}_{\text{clim}} + 2.5\,\text{K}$	1	50
SUSI_{EN}	$\text{SST}_{\text{clim}} + \text{SST}_{\text{EN}} + 2.5\,\text{K}$	20	2
$\text{SPSI}_{\text{ctrl}}$	$\text{SST}_{\text{clim}} + \text{SST}_{\text{SPSI}}$	1	50
SPSI_{EN}	$\text{SST}_{\text{clim}} + \text{SST}_{\text{EN}} + \text{SST}_{\text{SPSI}}$	20	2

Sea Surface Temperature, version 3b (ERSST.v3b), dataset (Smith et al. 2008) for the winter season (DJF) during 1949–2008. For monthly precipitation rate, we employ the National Oceanic and Atmospheric Administration's (NOAA) precipitation reconstruction dataset (Chen et al. 2002). Monthly mean 200-mb geopotential height, surface air temperature, and sea level pressure (SLP) from the National Centers for Environmental Prediction–National Center for Atmospheric Research (NCEP–NCAR) reanalysis are used (Kalnay et al. 1996).

To investigate the response of ENSO teleconnections to global warming, we divide the data into two periods of 1949–78 and 1979–2008. Linear regression is used to calculate DJF ENSO teleconnections (precipitation, geopotential height, SLP, and air temperature) for the two periods against the Niño-3 SST index (calculated in each period), defined as the average over 5°S–5°N, 150°–90°W. See Trenberth (1997) for more information on El Niño indices.

b. CAM4 experiments

CAM4 is the seventh-generation AGCM developed with significant community collaboration at the National Center for Atmospheric Research (NCAR). CAM4 is the atmospheric component of the Community Climate System Model, version 4 (CCSM4; Gent et al. 2011). A more comprehensive description of CAM4 can be found in Neale et al. (2011). The model uses a finite-volume core (Lin 2004) compared to the spectral core in CAM3. We choose a 1.9° × 2.5° grid (f19_f19) in the horizontal and 26 sigma levels in the vertical. Table 1 summarizes the experiments conducted.

A composite El Niño based on the average of four El Niño events of 1972/73, 1982/83, 1997/98, and 2009/10 is constructed. These cases were selected for their large magnitudes. We impose SST anomalies associated with the El Niño composite over a 2-yr period that begins before the El Niño event starts and concludes after the El Niño event has decayed. Specifically, the composite SST anomalies evolve from January of the El Niño developing year (year 0) to December of the decay year (year +1). The composite El Niño anomalies are added globally to the climatological SST for each month from January of year 0 through December of year +1. For convenience, the monthly climatology is the 1850–2008 average attached with CAM4. This climatology is used as the basic state for all the CAM4 experiments. Three pairs of integrations are performed, with the following SST boundary condition: 1) Present, the present climatology with and without the composite El Niño SST anomaly ("Present" pair in figures); 2) SPSI, as in Present but for a future basic state SST that is the present climatology plus a spatially patterned SST increase over the globe; and 3) SUSI, as in Present but for a basic state SST that is the present climatology plus a spatially uniform SST increase of 2.5 K over the globe (approximately equal to the 25°N–25°S mean of the SPSI in the second run). The SPSI is derived from the CCSM4 representative concentration pathway (RCP) 8.5 run as years 2081–2100 mean minus years 1986–2005 (historical run) mean (Fig. 1a). We use the difference between each pair to diagnose ENSO teleconnections under different basic states. We run the control experiment in each pair for 50 years, and use the control experiment to initialize the El Niño experiment. Each El Niño experiment has 20 members, each member lasting 2 years from January of year 0 to December of year +1. The radiative forcing (e.g., CO_2) levels are kept constant throughout all of the experiments. The 20-member ensemble average is used for analysis to reduce atmospheric internal variability.

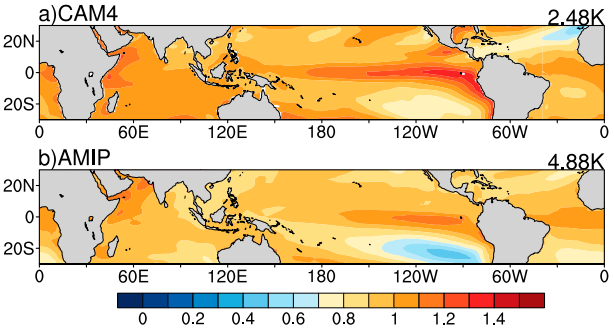

FIG. 1. Tropical SST warming (K) patterns derived from (a) years 2081–2100 (RCP 8.5 experiment) mean minus years 1986–2005 (historical run) mean in CCSM4, and (b) CMIP3 multimodel ensemble 4 × CO_2 experiment minus preindustrial control experiment, normalized by the respective tropical-mean values (25°N–25°S, marked at the upper-right corner).

c. AMIP ensemble

To test the robustness of the results, we analyze three additional sets of atmospheric experiments following the Atmospheric Model Intercomparison Project (AMIP) protocol (Gates et al. 1999) from the CMIP5 multimodel

ensemble available from the Program for Climate Model Diagnosis and Intercomparison (PCMDI). The three AMIP experiments are forced by observed SST evolution for 1979–2008 (the control run, known in CMIP5 terminology as "amip," all lowercase to distinguish it from the project), plus a spatially uniform SST increase of 4 K over all of the globe ("amip4K" in CMIP5) and a globally spatially patterned SST increase (Fig. 1b) derived from CMIP3 multimodel ensemble quadruple CO_2 (1% to 4×) simulations ("amipFuture"). The SPSI is scaled to have the same global mean SST as amip4K. The same ENSO events are embedded in these experiments (amip, amip4K, and amipFuture), which differ only in SST climatology. We use the linear regression method described in section 2a to calculate ENSO teleconnections. A total of 11 AGCMs are available (see Table 2, which includes expansions of model names). Only one member run is available for amip4K and amipFuture, limiting our ability to suppress atmospheric internal variability for individual models. The 11-model ensemble mean helps reduce internal variability. For consistency, we use only one member (r1i1p1) from each model for the control run. All model data are regridded to a common 2.5° × 2.5° grid prior to analysis.

Figure 1 shows the SST warming pattern from CCSM4 RCP8.5 and CMIP3 CO_2 quadrupling simulations, normalized by the respective tropical means. Despite the difference in warming magnitude, the normalized pattern is similar between the two, with an equatorial peak in the Pacific and Atlantic and a minimum in the southeast Pacific. This similarity also extends to the multimodel means of both CMIP3 and CMIP5, under a variety of future emissions scenarios (Power et al. 2013). The spatial variations are larger in CCSM4 as the multimodel average naturally smooths out spatial patterns. The maximum warming over the eastern equatorial Pacific exceeds 1.3 in CCSM4 as compared to the unit tropical mean, a pattern that substantially reduces the barrier to convection and is conducive for convection in the eastern Pacific during El Niño as shown in the next section.

TABLE 2. The 11 AMIP models analyzed in this study.

Model acronym	Expansion (institution)
BCC_CSM1.1	Beijing Climate Center, Climate System Model, version 1.1 (Beijing Climate Center, China)
CanAM4	Fourth Canadian Generation Atmospheric General Circulation Model (Canadian Centre for Climate Modelling and Analysis, Canada)
CCSM4	Community Climate System Model, version 4 (National Center for Atmospheric Research, United States)
CNRM-CM5	Centre National de Recherches Météorologiques (CNRM) Coupled Global Climate Model, version 5 (CNRM, France)
HadGEM2-A	Hadley Centre Global Environmental Model, version 2 (Atmosphere) (Hadley Centre, Met Office, United Kingdom)
IPSL-CM5A-LR	L'Institut Pierre-Simon Laplace (IPSL) Coupled Model, version 5A, coupled with Nucleus for European Modelling of the Ocean (NEMO), low resolution (IPSL, France)
IPSL-CM5B-LR	IPSL Coupled Model, version 5B, coupled with NEMO, low resolution (IPSL, France)
MIROC5	Model for Interdisciplinary Research on Climate, version 5 (Atmosphere and Ocean Research Institute, The University of Tokyo; National Institute for Environmental Studies; and Japan Agency for Marine-Earth Science and Technology, Japan)
MPI-ESM-LR	Max Planck Institute for Meteorology (MPI) Earth System Model, low resolution (MPI, Germany)
MPI-ESM-MR	MPI Earth System Model, medium resolution (MPI, Germany)
MRI-CGCM3	Meteorological Research Institute (MRI) Coupled Atmosphere–Ocean General Circulation Model, version 3 (MRI, Japan)

3. ENSO teleconnections in CAM4

We consider an idealized setting in which the tropical SST anomalies associated with El Niño undergo identical evolution in the Present run and the two warming scenarios of SPSI and SUSI. This isolates atmospheric processes for ENSO teleconnection changes under global warming. In the composite El Niño event, positive SST anomalies develop in the central Pacific in summer and fall, peak in winter of year 0, and then decay and develop into a La Niña event in year +1 (Fig. 2). We focus on the CAM4's response during the boreal winter season (December of year 0, January and February of year +1) when El Niño peaks.

Figure 3 (left) shows ENSO teleconnections for the present climate. The 200-mb geopotential height field (Fig. 3a) shows a PNA pattern (Wallace and Gutzler 1981) with two positive anomaly centers (>90 m) located in the subtropical Pacific near Hawaii and northern Canada, and two negative anomaly centers located in the North Pacific near the Aleutians (over −150 m) and the southeastern United States (over −60 m). For SLP (Fig. 3d), there are positive anomalies over the western tropical Pacific and negative anomalies over the eastern tropical Pacific, forming a zonal dipole of the Southern Oscillation. In the North Pacific, there is an anomalously deepened Aleutian low with the minimum value over

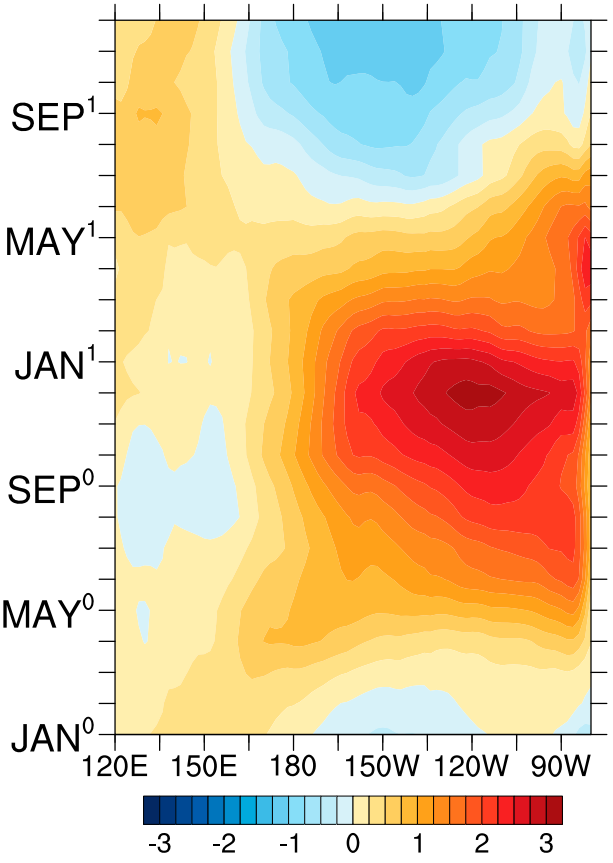

FIG. 2. Time–lon section of SST anomalies (K) in the composite El Niño event (5°N–5°S mean).

−12 mb. Positive SLP anomalies of over 6 mb are found over northeastern North America. El Niño causes precipitation to increase in the central and eastern equatorial Pacific of up to 8 mm day^{-1} with anomalous westerly winds. Over the North Pacific, precipitation increases on the south and eastern flanks of the anomalous Aleutian low. The intensified westerlies bring more precipitation to the southwestern United States but reduce precipitation over much of northern North America. For surface air temperature (Fig. 3j), the typical El Niño pattern of positive anomalies in the central and eastern equatorial Pacific is evident, with values over 2 K. Over North America, there are positive temperature anomalies of roughly +5 K over Canada and Alaska and negative anomalies of around −1 K over southern North America. There are negative surface temperature anomalies west of the Bering Strait due to the northerly advection by the anomalously deepened Aleutian low. The patterns of atmospheric anomalies in Fig. 3 are qualitatively similar to observations (Fig. 9, described in greater detail below) with some regional differences. Overall, the model captures major elements of the El Niño teleconnections.

a. Future changes

The El Niño–induced PNA teleconnection pattern remains dominant in the SPSI warming scenario but shows important differences from the Present simulation. In SLP, the anomalous Aleutian low deepens by 50%, with the minimum value at the center intensifying from −12 to over −18 mb (Figs. 3d,f). The center of the anomalous Aleutian low shifts northeastward by 20° longitude. The intensification and eastward shift of the anomalous Aleutian low are best illustrated in the SPSI minus Present difference of El Niño anomalies (Fig. 4a). The strengthening and eastward shift of the PNA pattern is also clear at 200 mb, especially at the North Pacific and northern Canada centers of action (Figs. 3a,c).

These changes in circulation anomalies cause considerable changes in surface temperature anomalies over land (Figs. 3g,i). El Niño–induced land surface warming is largely confined to Alaska in the Present run due to the warm advection by the anomalous southeasterlies. The land warming expands to cover almost entire North America north of Mexico in the SPSI run, a change due to the eastward shift of the anomalous Aleutian low. Despite a general relaxation of mean temperature gradient associated with the Arctic amplification, El Niño–induced North American warming intensifies in SPSI, a result of strengthened circulation anomalies. The eastward shift of the PNA pattern and the associated northerly advection cause a robust cooling over northeast Siberia west of the Bering Strait (Fig. 4c).

During El Niño winter, precipitation increases on the southern flank of the anomalous Aleutian low as the intensified westerlies (Fig. 3g) steer extratropical storms to more southerly positions. This band of precipitation increase intensifies and moves onshore toward North America due to the amplification and eastward shift of PNA circulation anomalies in SPSI future scenario (Fig. 3i). The intensified precipitation increase is most pronounced on and off the U.S. West Coast (Fig. 4b).

b. Causes of change: Tropical convection versus midlatitude flow

On the equator, the SPSI minus Present change in precipitation is positive east and negative west of the international date line while in the Present run, positive rainfall anomalies are found across the Pacific. Overall, the equatorial precipitation response to El Niño shows an intensification and eastward shift in SPSI compared to Present (Fig. 4b), accompanied by a similar intensification and eastward shift of 850-mb zonal wind response to El Niño. This is consistent with previous studies (Chung et al. 2014; Power et al. 2013). The intensification and eastward shift of

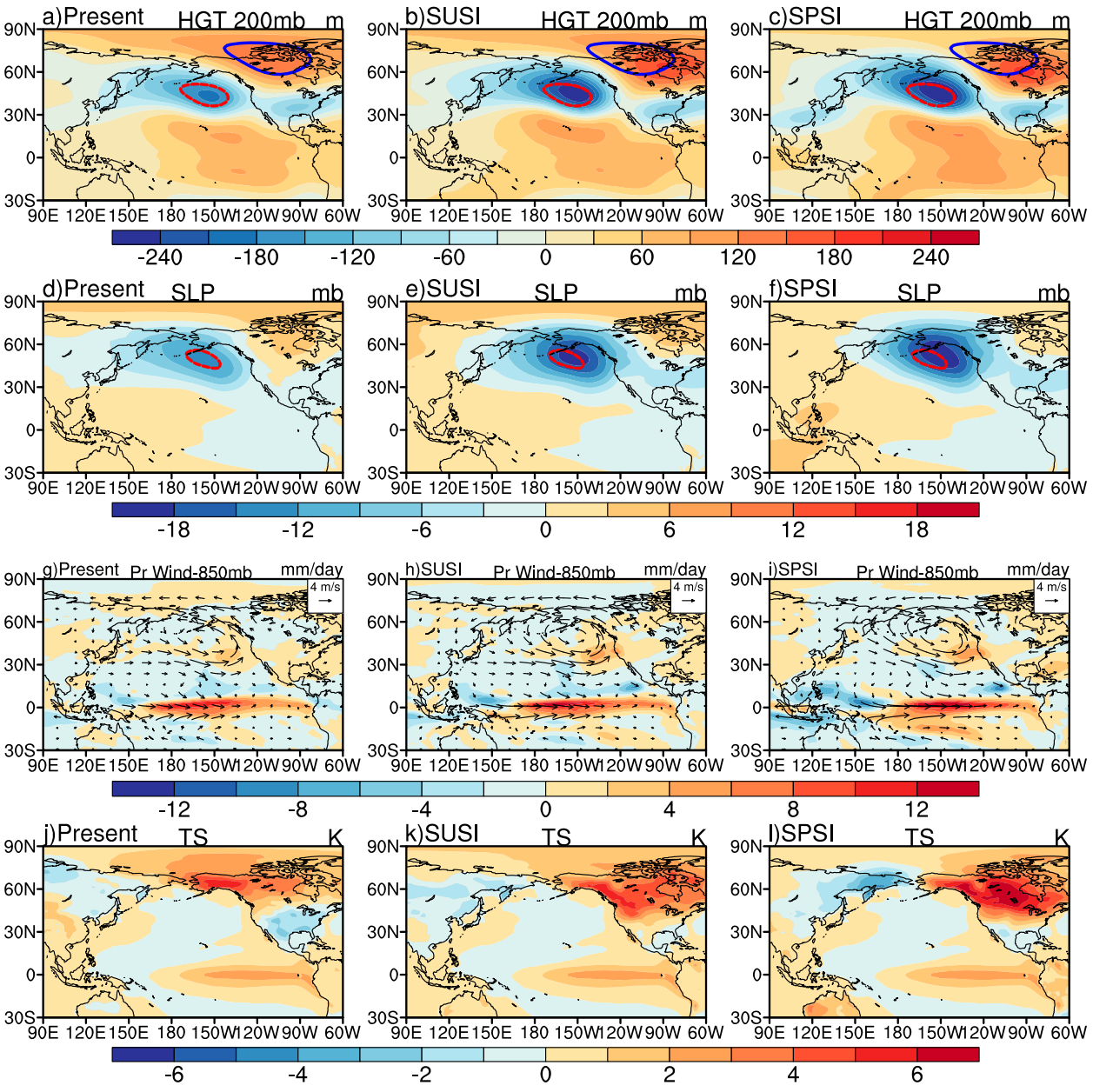

FIG. 3. The 20-member ensemble-mean anomalies of El Niño for DJF: 200-mb geopotential height (m), SLP (mb), precipitation (mm day^{-1}), 850-mb wind velocity (m s^{-1}), and surface temperature (K) in three scenarios in CAM4. The units are noted at the upper right, scaled to unit Niño-3 SST index. Red lines denote centers of action for SLP and geopotential height anomalies in the present climate.

El Niño–induced convective anomalies are a possible cause of similar changes in the PNA teleconnection pattern in SPSI future scenario.

There is an SST threshold for tropical convection, and this threshold is set by the tropical-mean SST, currently at 27 K. SST in the eastern equatorial Pacific is about 25 K for DJF, 2 K below the SST threshold. Only during major El Niño events as in 1997/98 does SST exceed the threshold and deep convection expand to the eastern equatorial Pacific. In SPSI, the SST warming is large over the eastern equatorial Pacific (Fig. 1a), exceeding the tropical mean by 0.75 K and reducing the barrier to the SST threshold by the same amount. (The SST threshold increases in step with the tropical-mean warming; Johnson and Xie 2010.) As a result, with the El Niño SST anomalies unchanged, eastern Pacific rainfall response to El Niño strengthens in a warmer climate (Chung et al. 2014; Power et al. 2013; Cai et al. 2014).

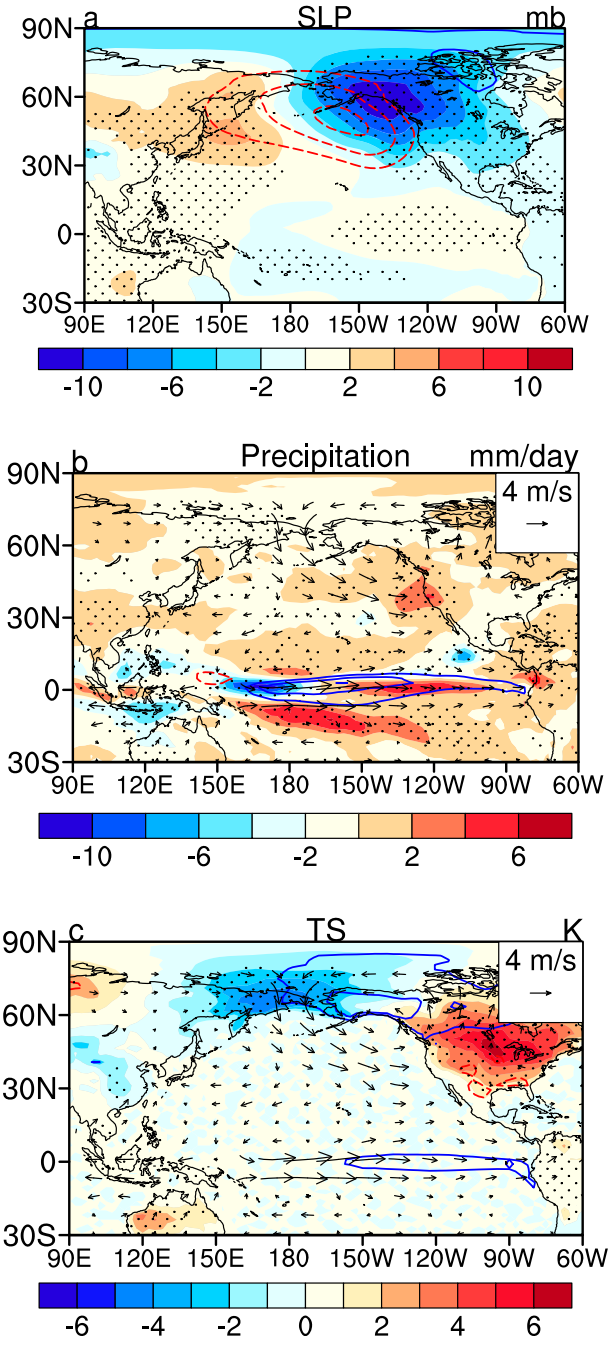

FIG. 4. Differences of (a) SLP (shading; mb), (b) precipitation (shading; mm day^{-1}), and (c) TS (shading; K) anomalies of El Niño between the Present and SPSI runs. Vectors showing 850-mb wind (m s^{-1}) are given in (b),(c). Colored lines denote key contours in the Present run (dashed red lines denote negative values and solid blue lines positive). Stippling indicates where the 20-member ensemble-mean differences are statistically significant at the 95% confidence level. The significance of the 20-member ensemble-mean differences is evaluated using a two-tailed Student's t test to test the null hypothesis that the sample means are from the same population (i.e., no difference).

In addition to tropical forcing, changes in the tropospheric mean flow in the midlatitudes can influence stationary waves like the PNA (Branstator 1984; Kang 1990; Meehl and Teng 2007). Stationary waves tend to shift eastward during periods of a strong zonal mean flow and vice versa. The warming in the tropical troposphere follows a moist adiabat and intensifies upward. As a result of strengthened poleward temperature gradient in the troposphere, the subtropical westerly flow (Fig. 5) accelerates. To test the effect of the westerly acceleration, we examine internal variability of the atmosphere. Even without tropical forcing, the PNA pattern arises spontaneously as an internal mode due to zonal variations in the mean flow (Simmons et al. 1983; Mori and Watanabe 2008). We have performed an empirical orthogonal function (EOF) analysis over the PNA region (0°–90°N, 120°E–60°W) based on the 50-yr CAM4 control runs with the repeating SST climatology for the present and SPSI climates. Figure 6 shows the leading modes of 200-mb geopotential height variability. The first EOF mode (Figs. 6a,b) is the internal PNA pattern, explaining about 40% of variance. The second EOF mode (Figs. 6c,d) is the annular mode, explaining about 20% of variance. Hereafter, we call the PNA pattern during El Niño winters the forced mode to distinguish from the internal PNA mode that develops spontaneously without tropical SST forcing.

The internal PNA mode qualitatively resembles the El Niño–forced PNA but differs considerably in geographical locations of action centers. The most striking difference is in the tropics, with little signals for the internal PNA (Figs. 6a,b) but large anomalies in the forced PNA mode (Figs. 3a–c and 7a,b). The subtropical center of action is also very different, displaced far west of Hawaii for the internal PNA and east of Hawaii for the forced mode. Overall the internal PNA mode does not show a substantial eastward shift before and after warming: although the Aleutian center of action shifts southeastward, the Canadian center of action shifts westward. The lack of a systematic eastward shift for the internal PNA mode suggests a limited effect of the accelerated midlatitude westerlies on the changes of the PNA teleconnection. The migration of El Niño–induced tropical convective anomalies appears important for the eastward shift of ENSO teleconnections before and after the climate warming.

In the SUSI run, the anomalous Aleutian low intensifies and moves slightly eastward, accompanied by moderate changes in the tropics (Fig. 3, middle). Overall, changes in atmospheric anomalies of El Niño are more pronounced in SPSI than SUSI, illustrating the importance of the mean SST warming pattern for interannual

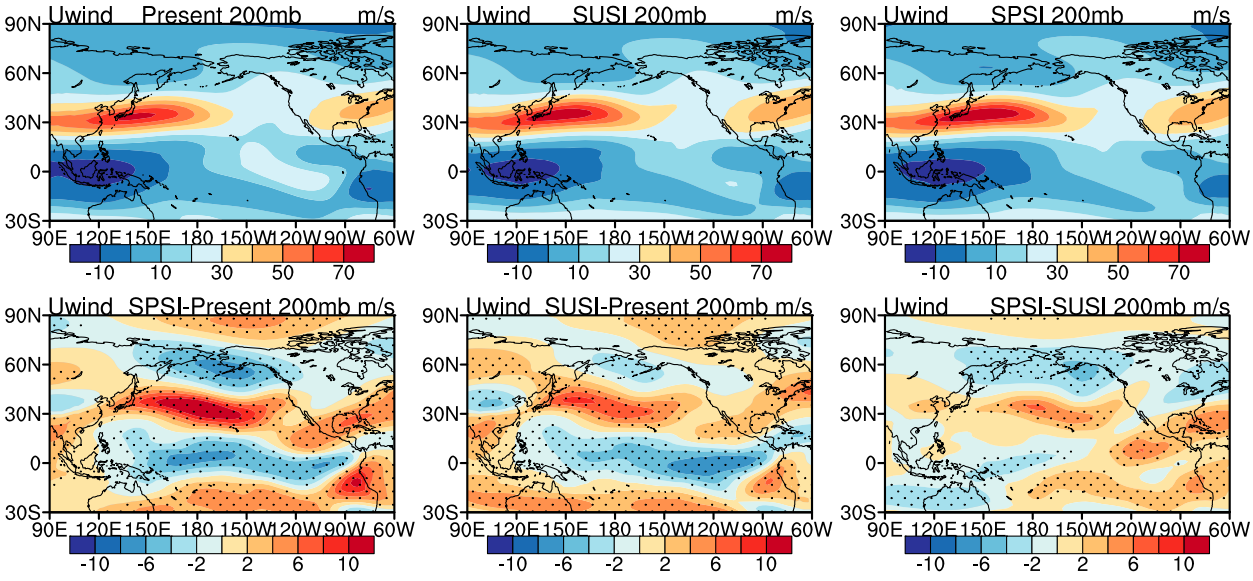

FIG. 5. DJF basic state zonal flow ($m\,s^{-1}$) at 200 mb in three control experiments and their differences. Stippling indicates regions exceeding 95% statistical confidence.

variability (e.g., through reducing the barrier of eastern Pacific SST to the convective threshold).

4. Atmospheric multimodel ensemble

We now turn to three sets of multimodel AMIP experiments in the CMIP5 archive (amip, amip4K, and amipFuture) to diagnose ENSO teleconnection changes under global warming, a novel use of AMIP runs. The SST warming pattern in amipFuture is smoother and weaker than that derived from CCSM4 for the CAM4 SPSI experiment (Fig. 1). Figure 7 presents the regression analysis of ENSO-induced atmospheric anomalies for the DJF season. The regression fields are very similar to our

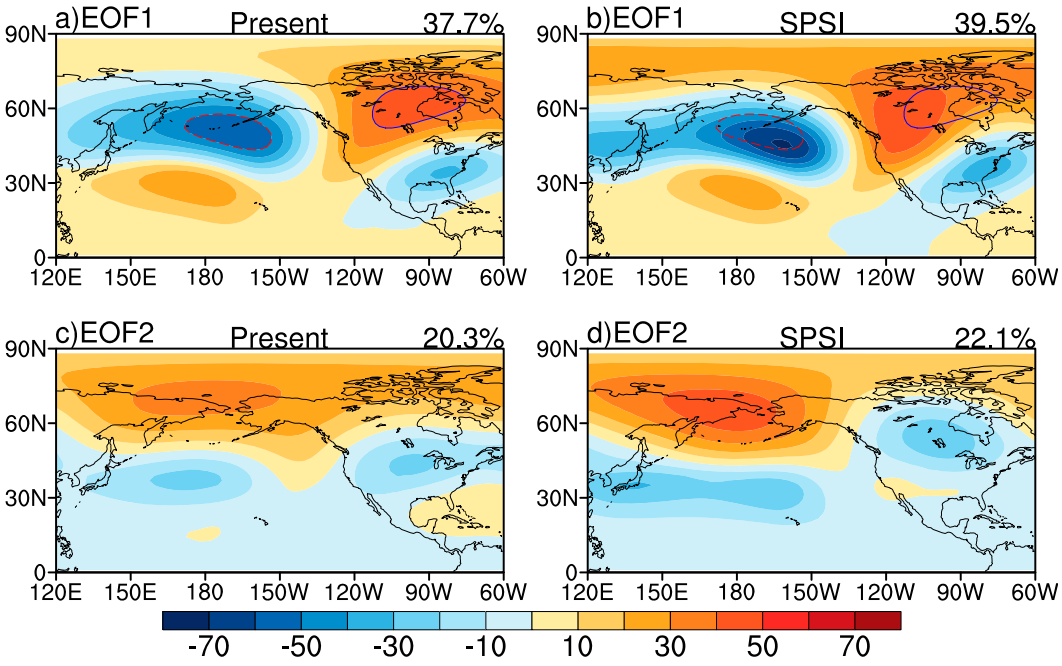

FIG. 6. (top) First and (bottom) second EOF modes of internal variability in 200-mb geopotential height in 50-yr-long (a),(c) Present and (b),(d) SPSI control experiments. Colored lines denote the center of action in the Present run (dashed red lines denote negative values and solid blue lines positive values).

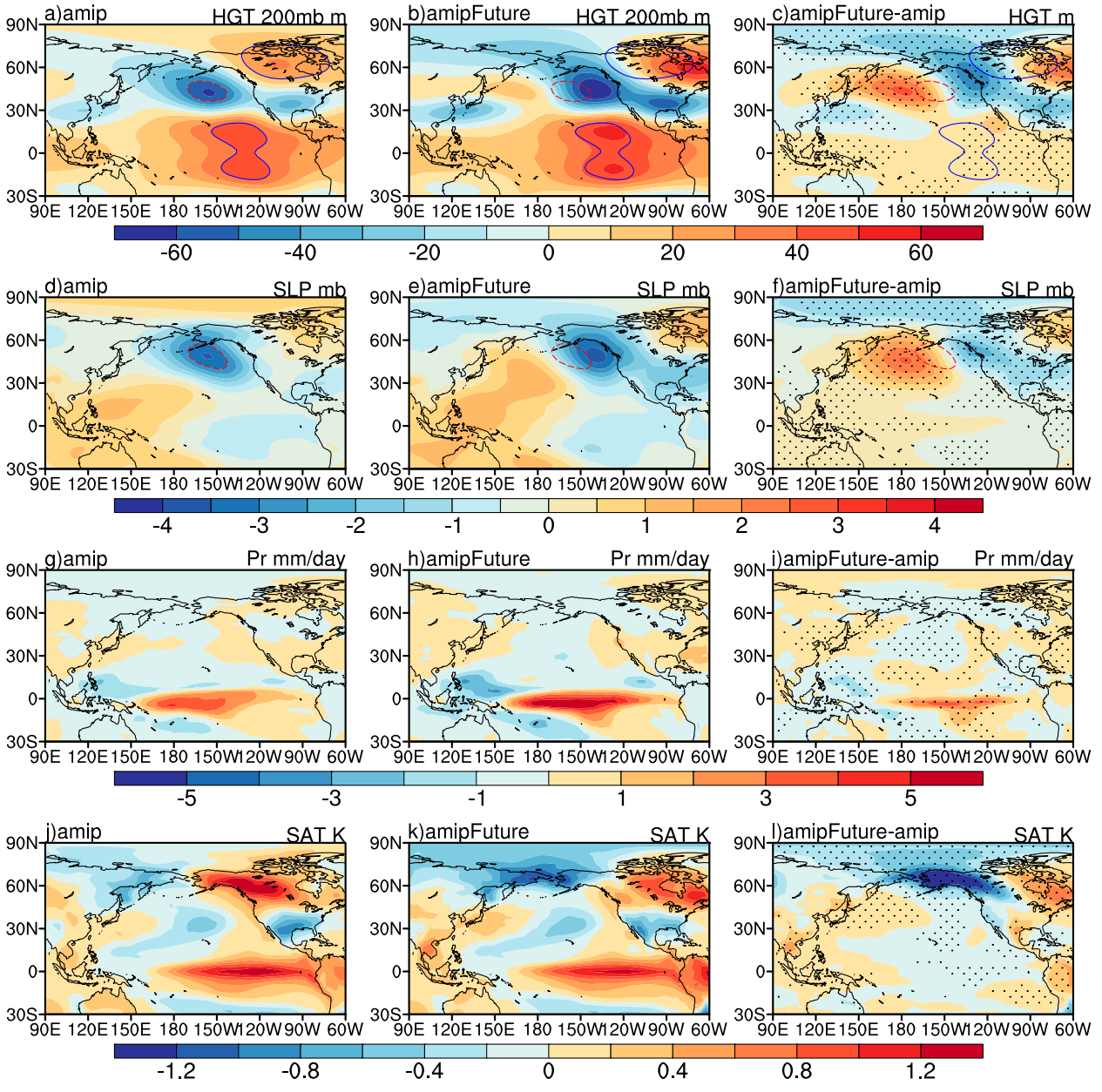

FIG. 7. As in Fig. 3, but for 11-model AMIP ensemble-mean regression coefficients upon the Niño-3 SST index. The difference between amipFuture and amip experiments is given at (right). Stippling indicates regions exceeding 95% statistical confidence. Dashed red lines denote negative values and solid blue lines positive values.

CAM4 experiments except that the magnitudes are scaled for unit Niño-3 SST index in the multimodel AMIP simulations. In the amipFuture run, the enhanced mean warming in the eastern equatorial Pacific causes a systematic eastward shift and enhancement of the atmospheric convection anomaly pattern of El Niño (Figs. 7g,i). In the 200-mb geopotential field, this change in tropical forcing strengthens the PNA pattern, and causes an eastward shift of the Aleutian and Canadian centers of action. A northeastward-oriented wave train over East Asia strengthens in amipFuture runs, possibly due to the decreased precipitation in the tropical western Pacific (Zheng et al. 2013).

In SLP, the eastward migration of the anomalous Aleutian low is clear in the amipFuture scenario but the intensification is not (Figs. 7d,e). The lack of the intensification could be due to the multimodel average as the center of the anomalous low varies in location among models (Fig. 8c).

Figure 8 (left) compares the central longitudes of enhanced tropical convection and the anomalous Aleutian

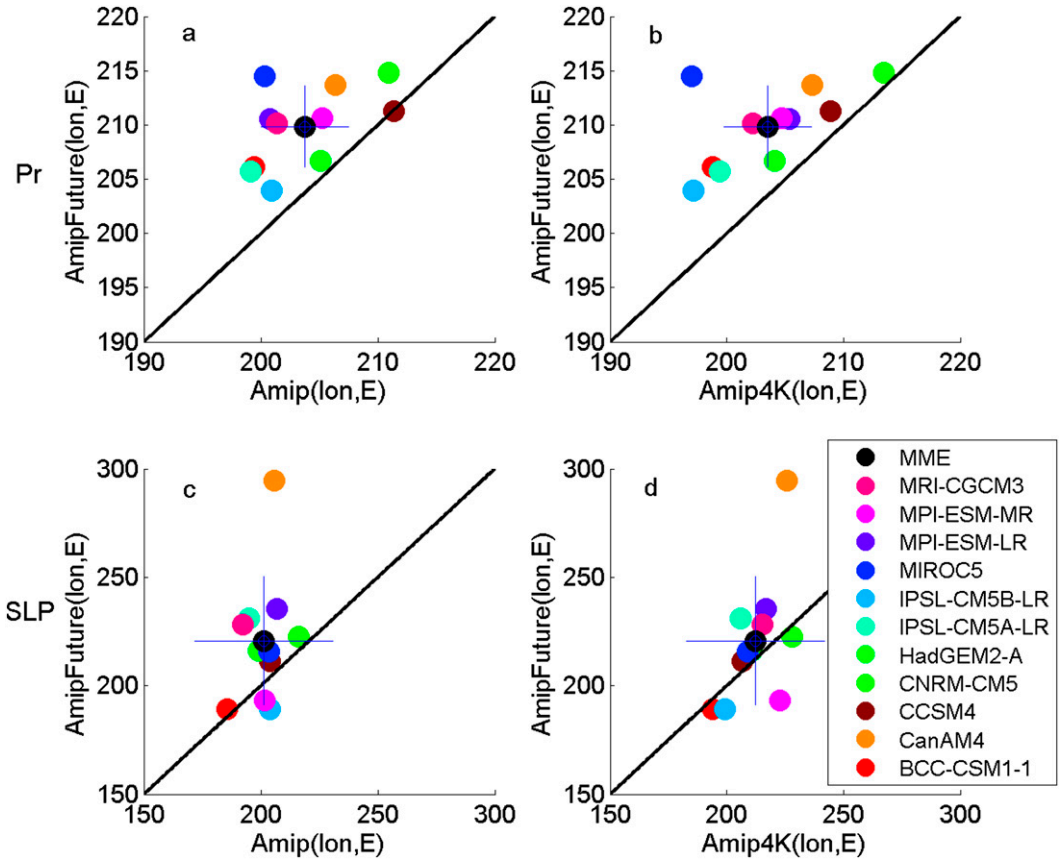

FIG. 8. Scatterplots for the central lon of tropical Pacific precipitation increase (Pr) and the anomalous Aleutian low between amip, amip4K, and amipFuture among 11 AMIP models. The black dot and error bars denote the ensemble mean and std dev of intermodel variability, respectively.

low during El Niño between amip and amipFuture. The anomalous tropical convection center is the centroid of El Niño–induced precipitation increase greater than 1 mm day^{-1} in the equatorial Pacific (10°S–10°N, 90°E–60°W), while the center of the anomalous Aleutian low is defined as the centroid of SLP anomalies exceeding −2 mb in the North Pacific (30°–90°N, 90°E–60°W). Compared to the present climate, the tropical convection shifts eastward consistently in all but one model, and the anomalous Aleutian low migrates eastward in all but two models in amipFuture. In the ensemble mean, the eastward shift amounts to 8° for tropical convection and 20° for the North Pacific SLP. The eastward shift in the anomalous Aleutian low under global warming takes place for both eastern and central Pacific El Niño events (see the appendix).

The eastward shift of El Niño–induced tropical convection is consistently more pronounced in amipFuture than amip4K, illustrating the effect of the patterned warming in the mean state (Fig. 8b). Chung et al. (2014) also showed that the precipitation response to El Niño in a warm climate depends on the structure of the imposed global warming SST pattern in the mean. The enhanced eastward migration of the North Pacific SLP anomalies from amip4K and amipFuture is less clear but more than half the models show this tendency (Fig. 8d), a result that one should not read too deeply into as it is based on a single 30-yr run for each model that includes internal atmospheric variability. Our analysis in section 3 suggests that the eastward shift of tropical convective anomalies affects the El Niño atmospheric teleconnections around the globe. A rigorous test of the hypothesis requires multiple realizations to evaluate the PNA response to global warming in individual models.

The eastward migration of the PNA in amipFuture has large impacts on surface temperature and precipitation response to El Niño (Fig. 7). The El Niño warming located over northwestern North America in amip moves to northeastern North America in amipFuture. The change is most dramatic over Alaska, with the warming replaced by a cooling. The warming over Japan and the South China Sea (Liu et al. 2004) also intensifies in amipFuture in the western Pacific. In

precipitation, the El Niño–induced increase strengthens in amipFuture on the U.S. West Coast, consistent with the CAM4 experiments.

5. Observed teleconnection changes

Are there any hints from observations that the El Niño–induced PNA shifts eastward in a warmer climate? To investigate ENSO teleconnection changes over the recent 60 years when the NCEP reanalysis is available, we divide data into two 30-yr periods of 1949–78 and 1979–2008. The two epochs correspond to the cold and warm phases of the interdecadal Pacific oscillation, respectively (Power et al. 1999; Deser and Phillips 2006). The tropical Pacific (10°N–10°S, 180°–80°W) is warmer by 0.37 K in the second than the first epoch. Figure 9 presents the regression analysis for the DJF season based on the Niño-3 SST index. Over the tropical Pacific, the El Niño warming is more sharply focused on the equator, and the precipitation increase extends farther eastward in the second epoch. The eastward migration of tropical convection reflects two mega El Niño events of 1982/83 and 1997/98. The anomalous Aleutian low deepens and shifts eastward into the Gulf of Alaska in the recent epoch (Hoerling et al. 1997). Associated with the circulation change, the El Niño–induced warming centered over Alaska moves southeastward.

The co-migration of tropical convection and the anomalous Aleutian low is suggestive of the former causing the latter. In model projections, the equatorially enhanced warming in the mean boosts the eastward migration of tropical convection (sections 3 and 4) but the SST warming pattern is somewhat uncertain in observations (Vecchi and Soden 2007; Tokinaga et al. 2012) because of measurement aliasing and sampling errors. A recent study suggested a weak equatorial enhancement over the past 60 years (Tokinaga et al. 2012). While the SST warming pattern strengthens the PNA change, the intensification and eastward migration of the anomalous Aleutian low, albeit weaker, take place even when the SST warming is uniform in space (SUSI runs). Thus, the PNA changes in the recent epoch may be due partly to climate warming, but natural variability in ENSO (Wittenberg 2009) and/or PNA (Deser et al. 2012) may also be important. Further detailed diagnostics will be executed in the future studies.

6. Summary and discussion

We have investigated changes in ENSO teleconnections in response to global warming in DJF in the Pacific–North American sector. An important deviation from previous studies is our use of AGCMs to isolate atmospheric processes and changes. Forced with the SST anomaly patterns of ENSO derived from observations, the AGCMs reproduce major atmospheric anomalies associated with El Niño, including a zonal dipole of precipitation anomalies on the equator and the PNA pattern. By holding the ENSO SST pattern identical for both the present and future climate simulations, we sidestep a major uncertainty in changes in ENSO properties such as amplitude and SST pattern (Collins et al. 2010; Christensen et al. 2013). When the spatial pattern of mean SST warming derived from coupled model projections is used, robust changes are found in El Niño–induced atmospheric anomalies in both the tropics and extratropics. In the tropics, the zonal dipole of precipitation intensifies and moves eastward as the enhanced equatorial warming in the mean state brings SST in the eastern Pacific closer to the convective threshold. The intensified precipitation increase during El Niño over the eastern equatorial Pacific is consistent with recent analyses of CMIP3 or CMIP5 simulations and SST-forced AGCM experiments (Chung et al. 2014; Power et al. 2013; Cai et al. 2014). In the extratropics, the PNA pattern in the upper troposphere and the anomalous Aleutian low in SLP during El Niño winters strengthen in magnitude and shift eastward. These changes are robust in an 11-model AMIP ensemble, with some support from observed changes from 1949–78 to 1979–2008, a 60-yr period during which tropical-mean SST in the Pacific (10°N–10°S, 180°–80°W) has risen by some 0.37 K.

This teleconnection response to global warming affects surface climate in the Pacific–North American sector. It is well known that during El Niño, surface temperature increases in northwestern North America centered at Alaska, and precipitation increases along the south flank of the anomalous Aleutian low as the intensified westerlies steer storms south. In a warmer climate, the eastward migration of the anomalous Aleutian low shifts these surface anomalies eastward. The El Niño–induced precipitation increase becomes more pronounced on the U.S. West Coast.

The above changes in atmospheric anomalies of El Niño are more pronounced when the SST warming features spatial variations rather than uniform increases. The center of El Niño–induced tropical rainfall increase consistently shifts eastward under SPSI compared to SUSI, illustrating the importance of enhanced warming in the eastern equatorial Pacific. The intensification and eastward shift of tropical forcing probably contribute to similar changes in the PNA teleconnection pattern through the Rossby wave mechanism. The differences in teleconnection pattern between central and eastern Pacific El Niño events corroborate the effect of tropical forcing. Compared to central Pacific El Niño, atmospheric

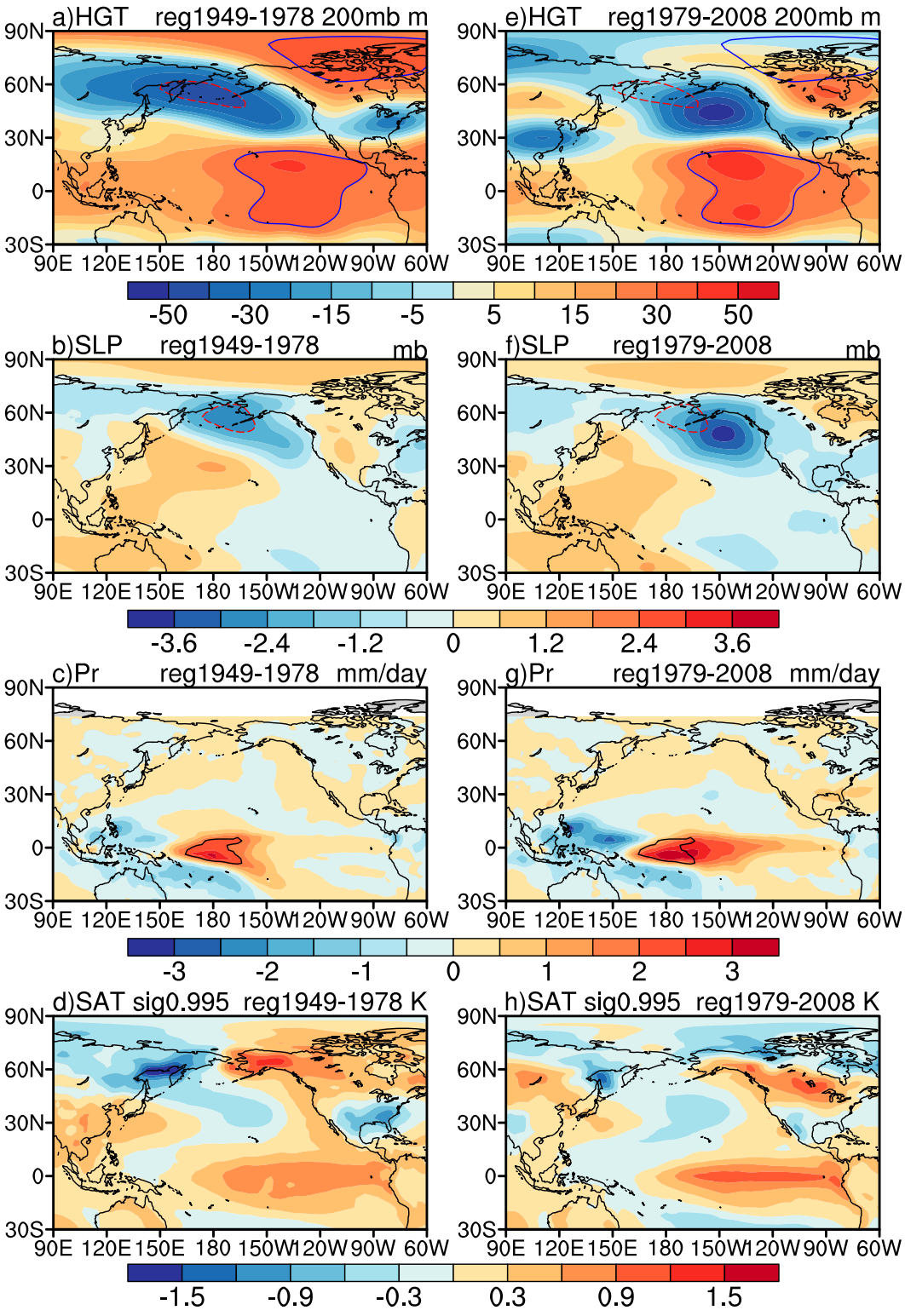

FIG. 9. As in Fig. 3, but for observed regressions upon the Niño-3 SST index for two 30-yr epochs. Colored lines denote key contours in (left) (dashed red lines denote negative values and solid blue lines positive values).

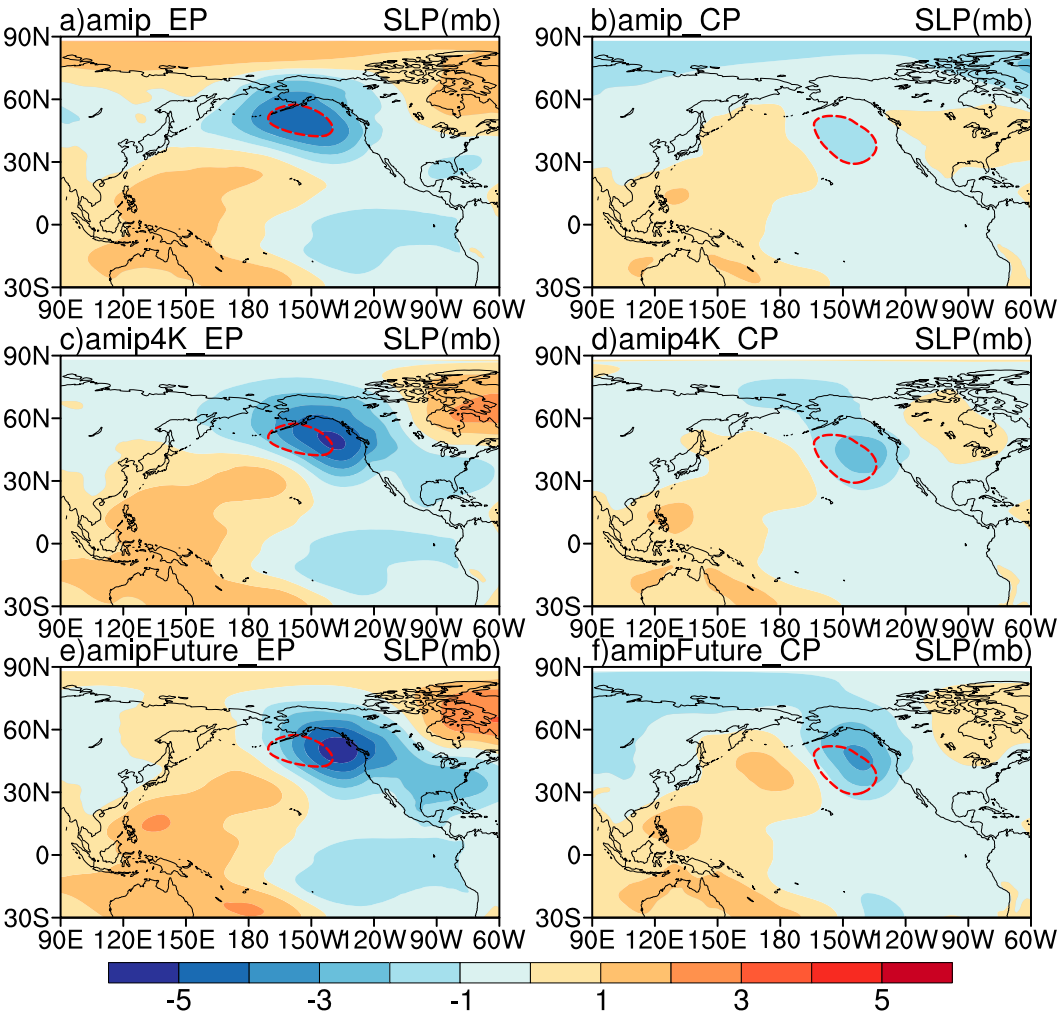

FIG. A1. Composites of atmospheric sea level pressure (SLP) anomalies for the DJF season for the (left) eastern and (right) central Pacific El Niño events (dashed red lines denote negative values).

anomalies over the North Pacific and North America shift eastward during eastern Pacific El Niño (Yu et al. 2012), associated with an eastward migration of tropical convective anomalies. These atmospheric changes are qualitatively similar to those in ENSO-induced atmospheric anomalies caused by global warming.

Even in SUSI where the change in tropical forcing is weak, the PNA pattern still shows an eastward shift, albeit weaker than in SPSI. This suggests that the acceleration of the subtropical westerly jet, a robust change insensitive to the SST warming pattern (Fig. 5) might also be important (e.g., Branstator 1984; Kang 1990). The changes in the midlatitude mean flow apparently do not have a strong effect on the PNA mode of atmospheric internal variability (Fig. 6). Further research is necessary to quantify the effects of tropical forcing and the midlatitude mean flow for ENSO teleconnection changes.

Acknowledgments. We acknowledge the WCRP Working Group on Coupled Modeling for producing and making CMIP5 output available; and the U.S. Department of Energy's Program for Climate Model Diagnosis and Intercomparison for providing the coordinating support and leading the development of software infrastructure in partnership with the Global Organization for Earth System Science Portals. We wish to thank Zedong Liu (OUC), Feng-Juan Cui (OUC), and Chao He (IAP) for helping set up CAM4. This work was supported by the National Basic Research Program of China (2012CB955600), the U.S. National Science Foundation, the Natural Science Foundation of China (41106010, 41176006, and 41476003), China Meteorological Public Welfare Scientific Research Project (GYHY201306027), and the 111 Project (B07036). Computational resources for CAM4 runs were provided by Computing Center of

the Key Laboratory of Physical Oceanography, Chinese Ministry of Education.

APPENDIX

Sensitivity to El Niño Types

We make composites for eastern Pacific and central Pacific El Niño events from the AMIP ensemble to see whether the magnitude of El Niño affects our results. Following Yu et al. (2012), we choose four eastern Pacific Niño events of 1982/83, 1986/87, 1997/98, and 2006/07, and five central Pacific Niño events of 1987/88, 1991/92, 1994/95, 2002/03, and 2004/05. Here we show the composites of DJF sea level pressure (SLP) anomalies for eastern Pacific and central Pacific El Niño events, respectively (Fig. A1). The results are similar to Yu et al. (2012): compared to central Pacific El Niño, the center of the anomalous Aleutian low shifts eastward for eastern Pacific El Niño (Fig. A1), associated with an eastward migration of tropical convective anomalies (not shown). Compared to the present climate (Figs. A1a,b), the eastward migration and intensification of the anomalous Aleutian low in the amipFuture scenario are evident for both types of El Niño events (Figs. A1e,f), accompanied by a systematic eastward shift and enhancement of the atmospheric convection anomaly in the tropical Pacific (not shown). As the amip and amipFuture runs differ only in the mean state, these results indicate that the above changes in atmospheric anomalies of El Niño are due to the mean state SST change and are insensitive to type or amplitude of ENSO.

REFERENCES

Branstator, G., 1984: The relationship between zonal mean flow and quasi-stationary waves in the midtroposphere. *J. Atmos. Sci.,* **41,** 2163–2178, doi:10.1175/1520-0469(1984)041<2163:TRBZMF>2.0.CO;2.

Cai, W., P. van Rensch, T. Cowan, and H. H. Hendon, 2011: Teleconnection pathways of ENSO and the IOD and the mechanisms for impacts on Australian rainfall. *J. Climate,* **24,** 3910–3923, doi:10.1175/2011JCLI4129.1.

——, and Coauthors, 2014: Increasing frequency of extreme El Niño events due to greenhouse warming. *Nat. Climate Change,* **4,** 111–116, doi:10.1038/nclimate2100.

Chadwick, R., I. Boutle, and G. Martin, 2013: Spatial patterns of precipitation change in CMIP5: Why the rich do not get richer in the tropics. *J. Climate,* **26,** 3803–3822, doi:10.1175/JCLI-D-12-00543.1.

Chen, M., P. Xie, J. E. Janowiak, and P. A. Arkin, 2002: Global land precipitation: A 50-yr monthly analysis based on gauge observations. *J. Hydrometeor.,* **3,** 249–266, doi:10.1175/1525-7541(2002)003<0249:GLPAYM>2.0.CO;2.

Christensen, J. H., and Coauthors, 2013: Climate phenomena and their relevance for future regional climate change. *Climate Change 2013: The Physical Science Basis,* T. F. Stocker et al., Eds., Cambridge University Press, 1217–1308.

Chung, C. T. Y., S. B. Power, J. M. Arblaster, H. A. Rashid, and G. L. Roff, 2014: Nonlinear precipitation response to El Niño and global warming in the Indo-Pacific. *Climate Dyn.,* **42,** 1837–1856, doi:10.1007/s00382-013-1892-8.

Collins, M., and Coauthors, 2010: The impact of global warming on the tropical Pacific Ocean and El Niño. *Nat. Geosci.,* **3,** 391–397, doi:10.1038/ngeo868.

Deser, C., and A. S. Phillips, 2006: Simulation of the 1976/77 climate transition over the North Pacific: Sensitivity to tropical forcing. *J. Climate,* **19,** 6170–6180, doi:10.1175/JCLI3963.1.

——, M. A. Alexander, S.-P. Xie, and A. S. Phillips, 2010: Sea surface temperature variability: Patterns and mechanisms. *Annu. Rev. Mar. Sci.,* **2,** 115–143, doi:10.1146/annurev-marine-120408-151453.

——, A. S. Phillips, V. Bourdette, and H. Teng, 2012: Uncertainty in climate change projections: The role of internal variability. *Climate Dyn.,* **38,** 527–546, doi:10.1007/s00382-010-0977-x.

Gates, W. L., and Coauthors, 1999: An overview of the results of the Atmospheric Model Intercomparison Project (AMIP I). *Bull. Amer. Meteor. Soc.,* **80,** 29–55, doi:10.1175/1520-0477(1999)080<0029:AOOTRO>2.0.CO;2.

Gent, P. R., and Coauthors, 2011: The Community Climate System Model version 4. *J. Climate,* **24,** 4973–4991, doi:10.1175/2011JCLI4083.1.

Hoerling, M. P., A. Kumar, and M. Zhong, 1997: El Niño, La Niña, and the nonlinearity of their teleconnections. *J. Climate,* **10,** 1769–1786, doi:10.1175/1520-0442(1997)010<1769:ENOLNA>2.0.CO;2.

Horel, J. D., and J. M. Wallace, 1981: Planetary-scale atmospheric phenomena associated with the Southern Oscillation. *Mon. Wea. Rev.,* **109,** 813–829, doi:10.1175/1520-0493(1981)109<0813:PSAPAW>2.0.CO;2.

Huang, P., S.-P. Xie, K. Hu, G. Huang, and R. Huang, 2013: Patterns of the seasonal response of tropical rainfall to global warming. *Nat. Geosci.,* **6,** 357–361, doi:10.1038/ngeo1792.

Johnson, N. C., and S.-P. Xie, 2010: Changes in the sea surface temperature threshold for tropical convection. *Nat. Geosci.,* **3,** 842–845, doi:10.1038/ngeo1008.

Kalnay, E., and Coauthors, 1996: The NCEP/NCAR 40-Year Reanalysis Project. *Bull. Amer. Meteor. Soc.,* **77,** 437–471, doi:10.1175/1520-0477(1996)077<0437:TNYRP>2.0.CO;2.

Kang, I.-S., 1990: Influence of zonal mean flow change on stationary wave fluctuations. *J. Atmos. Sci.,* **47,** 141–147, doi:10.1175/1520-0469(1990)047<0141:IOZMFC>2.0.CO;2.

Kug, J.-S., S.-I. An, Y.-G. Ham, and I.-S. Kang, 2010: Changes in El Niño and La Niña teleconnections over North Pacific–America in the global warming simulations. *Theor. Appl. Climatol.,* **100,** 275–282, doi:10.1007/s00704-009-0183-0.

Li, J., and Coauthors, 2013: El Niño modulations over the past seven centuries. *Nat. Climate Change,* **3,** 822–826, doi:10.1038/nclimate1936.

Lin, S. J., 2004: A "vertically Lagrangian" finite-volume dynamical core for global models. *Mon. Wea. Rev.,* **132,** 2293–2307, doi:10.1175/1520-0493(2004)132<2293:AVLFDC>2.0.CO;2.

Liu, Q., X. Jiang, S.-P. Xie, and W. T. Liu, 2004: A gap in the Indo-Pacific warm pool over the South China Sea in boreal winter: Seasonal development and interannual variability. *J. Geophys. Res.,* **109,** C07012, doi:10.1029/2003JC002179.

Ma, J., and S.-P. Xie, 2013: Regional patterns of sea surface temperature change: A source of uncertainty in future projections of precipitation and atmospheric circulation. *J. Climate,* **26,** 2482–2501, doi:10.1175/JCLI-D-12-00283.1.

McPhaden, M. J., S. E. Zebiak, and M. H. Glantz, 2006: ENSO as an integrating concept in earth science. *Science,* **314,** 1740–1745, doi:10.1126/science.1132588.

Meehl, G. A., and H. Teng, 2007: Multi-model changes in El Niño teleconnections over North America in a future warmer climate. *Climate Dyn.,* **29,** 779–790, doi:10.1007/s00382-007-0268-3.

Mori, M., and M. Watanabe, 2008: The growth and triggering mechanisms of the PNA: A MJO-PNA coherence. *J. Meteor. Soc. Japan,* **86,** 213–236, doi:10.2151/jmsj.86.213.

Neale, R. B., and Coauthors, 2011: Description of the NCAR Community Atmosphere Model (CAM4). NCAR Tech. Note NCAR/TN-485+STR, 120 pp.

Ogata, T., S.-P. Xie, A. Wittenberg, and D.-Z. Sun, 2013: Interdecadal amplitude modulation of El Niño–Southern Oscillation and its impacts on tropical Pacific decadal variability. *J. Climate,* **26,** 7280–7297, doi:10.1175/JCLI-D-12-00415.1.

Philander, S. G., Ed., 1990: *El Niño, La Niña, and the Southern Oscillation.* Academic Press, 293 pp.

Power, S., T. Casey, C. Folland, A. Colman, and V. Mehta, 1999: Inter-decadal modulation of the impact of ENSO on Australia. *Climate Dyn.,* **15,** 319–324, doi:10.1007/s003820050284.

——, F. Delage, C. Chung, G. Kociuba, and K. Keay, 2013: Robust twenty-first-century projections of El Niño and related precipitation variability. *Nature,* **502,** 541–545, doi:10.1038/nature12580.

Simmons, A. J., J. M. Wallace, and G. W. Branstator, 1983: Barotropic wave propagation and instability, and atmospheric teleconnection patterns. *J. Atmos. Sci.,* **40,** 1363–1392, doi:10.1175/1520-0469(1983)040<1363:BWPAIA>2.0.CO;2.

Smith, T. M., R. W. Reynolds, T. C. Peterson, and J. Lawrimore, 2008: Improvements to NOAA's historical merged land–ocean surface temperature analysis (1880–2006). *J. Climate,* **21,** 2283–2296, doi:10.1175/2007JCLI2100.1.

Stevenson, S. L., 2012: Significant changes to ENSO strength and impacts in the twenty-first century: Results from CMIP5. *Geophys. Res. Lett.,* **39,** L17703, doi:10.1029/2012GL052759.

Tokinaga, H., S.-P. Xie, C. Deser, Y. Kosaka, and Y. M. Okumura, 2012: Slowdown of the Walker circulation driven by tropical Indo-Pacific warming. *Nature,* **491,** 439–443, doi:10.1038/nature11576.

Trenberth, K. E., 1997: The definition of El Niño. *Bull. Amer. Meteor. Soc.,* **78,** 2771–2777, doi:10.1175/1520-0477(1997)078<2771:TDOENO>2.0.CO;2.

Vecchi, G. A., and B. J. Soden, 2007: Global warming and the weakening of the tropical circulation. *J. Climate,* **20,** 4316–4340, doi:10.1175/JCLI4258.1.

Wallace, J. M., and D. S. Gutzler, 1981: Teleconnections in the geopotential height field during the Northern Hemisphere winter. *Mon. Wea. Rev.,* **109,** 784–812, doi:10.1175/1520-0493(1981)109<0784:TITGHF>2.0.CO;2.

——, E. M. Rasmusson, T. P. Mitchell, V. E. Kousky, E. S. Sarachik, and H. V. Storch, 1998: On the structure and evolution of ENSO-related climate variability in the tropical Pacific: Lessons from TOGA. *J. Geophys. Res.,* **103,** 14 241–14 259, doi:10.1029/97JC02905.

Wittenberg, A. T., 2009: Are historical records sufficient to constrain ENSO simulations? *Geophys. Res. Lett.,* **36,** L12702, doi:10.1029/2009GL038710.

Xie, S.-P., C. Deser, G. A. Vecchi, J. Ma, H. Teng, and A. T. Wittenberg, 2010: Global warming pattern formation: Sea surface temperature and rainfall. *J. Climate,* **23,** 966–986, doi:10.1175/2009JCLI3329.1.

Yu, J.-Y., Y. Zou, S. T. Kim, and T. Lee, 2012: The changing impact of El Niño on US winter temperatures. *Geophys. Res. Lett.,* **39,** L15702, doi:10.1029/2012GL052483.

Zheng, J., Q. Liu, C. Wang, and X.-T. Zheng, 2013: Impact of heating anomalies associated with rainfall variations over the Indo-western Pacific on Asian atmospheric circulation in winter. *Climate Dyn.,* **40,** 2023–2033, doi:10.1007/s00382-012-1478-x.